Raman Imaging and Spectroscopy of Heterogeneous Individual Carbon Nanotubes

Chaoyang Jiang,[†,#] Jialong Zhao,[†] Helen A. Therese,[‡] Marcel Friedrich,[†] and Alf Mews*[,†]

Institut für Physikalische Chemie and Institut für Anorganische und Analytische Chemie, Universität Mainz, D-55099 Mainz, Germany

Received: May 19, 2003; In Final Form: July 4, 2003

Isolated single-walled carbon nanotubes (CNTs) were grown by chemical vapor deposition methods on Fe/Mo/Al_2O_3 catalysts, which were patterned by microcontact printing. The pattern allowed us to trace back and investigate the same isolated CNT by atomic-force (AFM) and confocal Raman microscopy with different excitation wavelengths. A change of the Raman intensity could be correlated with structural defects revealing that the molecular structure of the tubes is changing along the tube axis. By investigating the same tube segments with different excitation energies, we found that the D-line of isolated tubes shows a strong dispersive effect of 45−50 cm^{-1}/eV. In contrast, the spectral position of the G-line shows no frequency shift with changing excitation energy but is different for various tube segments.

Introduction

The electronic properties of carbon nanotubes (CNTs) are directly related to their atomic structures. Because an ideal CNT can be viewed as a rolled up segment of a graphene sheet, the roll up geometry can lead to many different CNTs with numerous symmetries and diameters.[1] Essentially, each of those tubes has a different electronic structure,[2] which makes an ensemble of CNTs a highly inhomogeneous system. In addition, most large-scale production methods lead to bundles of CNTs with possible intrabundle interaction,[3] which further complicates a detailed investigation of the electronic properties and hampers the development of electronic devices based on CNTs.

A big step forward in the direction of reliable device fabrication has been the development of chemical vapor deposition (CVD) techniques to grow individual tubes. Several attempts have been performed to control the diameter and the length of the tubes.[4,5] Also it was shown that the growth position can be adjusted by patterning the catalysts[6] and even the growth direction could be tuned by applying an electric field during the growth process.[7]

However, even though single isolated tubes are now available, the structure and therefore the electronic properties of a particular CNT can change along the tube axis because of structural defects, which can be experimentally observed by scanning tunneling microscopy (STM).[8] On the other hand, the high resolution of STM allows only a limited scan range and the investigation of very long CNTs (greater than several micrometers) can hardly be performed. Another powerful microscopic technique for the imaging and spectroscopy of CNTs is the method of scanning confocal microscopy in which individual CNTs or small bundles can be localized by their very strong Raman signal[9,10] and spectra can be taken with different excitation energies.[11,12] The spatial resolution in conventional confocal Raman imaging is given by the natural diffraction limit (approx. $\lambda/2$) but can be increased significantly with near-field techniques, as has been shown recently.[13]

Because a change of the structural properties is correlated with a change of the electronic structure the Raman intensity can change along the tube axis. This is a direct result of the selective resonance conditions in Raman spectroscopy in which the Raman signal is strongly enhanced if, in the simplest case, either the incoming excitation photon or the scattered photon is in resonance with an electronic transition.[14] On the basis of this interpretation, which is called a "single-resonance Raman process", several characteristic features of individual CNTs, such as diameter and chirality,[15,16] and also the electronic densities of state have been investigated.[17]

A different interpretation of the Raman enhancement process is based on a so-called "double-resonance Raman process". Briefly, the single-resonance process is based on the assumption that only Γ-point modes ($q \approx 0$) contribute to the scattering and therefore the frequency of the modes should not depend on the excitation energy. In contrast, the double-resonance theory is based on the idea that local defects within the tubes allow for optical transitions throughout the whole *k*-space and therefore enhancement of different phonon modes.[18] While this interpretation is commonly accepted for the disorder-induced D-line at about 1350 cm^{-1},[19−21] it is still under investigation whether the graphite-like G-line around 1590 cm^{-1} can be explained by single-[22] or double-resonance Raman effects.[23] Experimental evidence as to which model might hold could be given by Raman spectroscopy of the same isolated CNT with different excitation energies, because Raman modes that derive from a double-resonance process should change with excitation energy, whereas the modes that originate from a single-resonance effect should not show this dispersive effect.

In this letter, we will investigate the same isolated CNTs in a broader excitation energy range as that in ref 22. First, we will present a CVD scheme in which the catalyst is patterned by microcontact printing such that the same tube can be investigated by atomic-force microscopy (AFM) and confocal Raman microscopy and spectroscopy. We will show that different parts of a single CNT light up at different excitation energies as a consequence of structural changes along the tube

* To whom correspondence should be addressed. E-mail: alf.mews@uni-mainz.de.
† Institut für Physikalische Chemie.
# Present address: Department of Materials Science & Engineering, Iowa State University, Gilman Hall, Ames, IA 50011.
‡ Institut für Anorganische Chemie und Analytische Chemie.

10.1021/jp035371r CCC: $25.00
Published on Web 08/05/2003

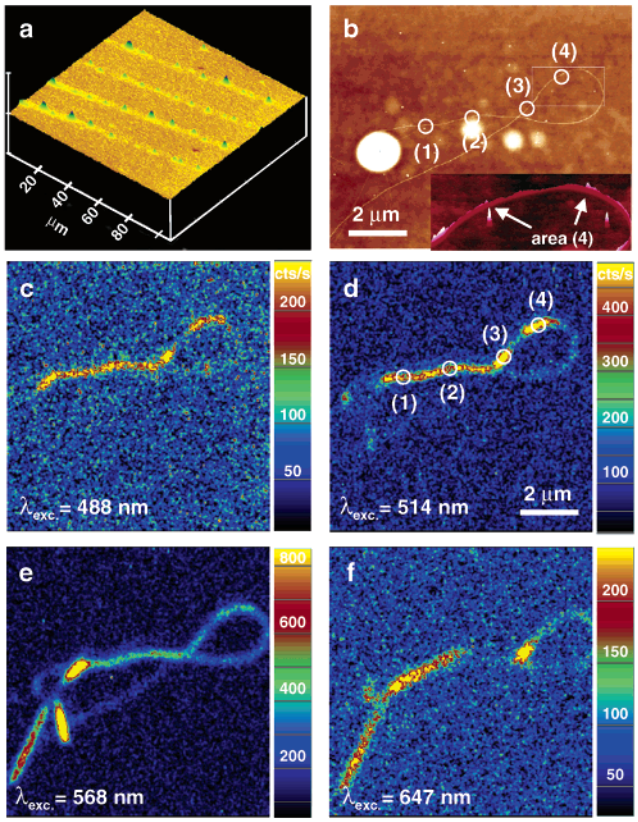

Figure 1. Imaging of individual CNTs: (a) optical image of the silicon substrate with catalyst pattern as deposited by microcontact printing technique; (b) AFM of individual CNTs (thin lines) that grew from a porous catalyst structure (bright spot). The circles mark the positions (1−4) at which the Raman spectra were taken with different excitation wavelength. The inset shows the 3-D AFM in the range of area 4 where the arrows point at "nano particular defects" within the tube. Panels c−f show scanning confocal Raman images based on the G-line intensity and taken with four different excitation wavelengths. The Raman intensity is changing between and within individual tubes.

axis. The different "CNT segments" are investigated by four different excitation energies, and the Raman spectra in the range of the D- and G-lines are compared.

Experimental Section

The isolated CNTs were obtained by CVD growth on microprinted Fe/Mo/Al_2O_3 catalyst structures similar to the method developed by Gu et al.[24] Briefly, a drop of the catalyst solution was placed on the poly[dimethylsiloxane] (PDMS) stamp, which was subsequently dried in air and gently put on a silicon wafer for 10 s. Then the substrate was annealed in air for 10 h at 500 °C, which leads to a decomposition of the block copolymer leaving behind the catalyst in a regular pattern of porous structures.[25] Because the stamp consists of a linear array of four lines with a distance of 25 μm, this results in lines of porous catalyst aggregates, which can easily be seen in an optical microscope as shown in Figure 1a. Before the tube growth, the substrate with the deposited catalyst was first calcinated under argon and activated with a mixture of argon and hydrogen at 950 °C. For the actual growth, the argon was replaced by methane for 30 min, after which the substrate was cooled to room temperature under pure argon flow.

The AFM images were taken with a Nanoscope IIIa system (Digital Instruments) using commercial Si_3N_4 tips and tapping mode. Raman imaging and spectroscopy was performed with a home-built confocal Raman microscope as described elsewhere.[9] Here we used four different lines (488, 514.5, 568.2, and 647.1 nm) from an Ar−Kr ion laser, which were circularly polarized and adjusted to an excitation intensity of 1 MW/cm^2 in the center of the diffraction-limited excitation spot. The images and spectra were recorded for 10−20 min and 10−30 min, respectively. All images are based on the G-line of the CNTs, that is, while the sample is scanned through the excitation spot, only the spectral range of 1590 ± 15 cm^{-1} is guided to an avalanche photodiode (APD) and the photon count rate at each position is plotted (Figure 1c−f). After the image was taken, the positions 1−4 in Figure 1 were subsequently moved in the center of the excitation spot, and the spectra were recorded with a liquid nitrogen cooled CCD camera.

Results and Discussions

Figure 1b shows an AFM image of one loop-shaped and several shorter CNTs, which obviously start from catalyst particles within the porous structure that can be seen as a bright spot. The diameter distribution was determined from the height profiles of about 100 tubes to be in the range between 1 and 4 nm in correspondence with the observed diameter distribution in ref 24. In that paper, it has also been shown by TEM measurements that the described growth conditions lead to single-wall CNTs and not to bundles or multiwall CNTs. The AFM height along the loop-shaped CNT is in the range of 2 ± 0.5 nm, while some "nanoscopic particles" with a height of up to 7 nm appear along the tube as shown, for example, in the inset of Figure 1b (arrows).

Because the large porous catalyst structure could be easily traced back in the optical microscope, the corresponding Raman images of the same tubes can be taken with different excitation wavelengths (Figure 1c−f). Obviously several tubes and various sections within each tube lighten up at different excitation energies as a consequence of the changing electronic structure along the tube axis. In some cases, the Raman intensity changes dramatically even though the height does not change within the accuracy of the AFM measurement, which is mainly determined by the surface roughness (<0.3 nm). In other cases, the Raman intensity changes at the position of the nanoscopic particles, as seen by comparison of the inset in Figure 1b with the corresponding Raman images. While this work was being completed, Hartschuh et al. reported similar results by tip-induced near-field Raman microscopy, in which the bumps were tentatively attributed to remaining catalyst particles.[13] However, the origin of those structures is still not known and will be subject of further investigations.

In any case, the uniformity of the Raman intensity along one specific tube is a direct measure of the "electronic homogeneity" of that tube. In this letter, we will focus on the Raman spectroscopy of different tube segments by investigating the CNT shown in Figure 1 at four different spots (1−4). First it should be mentioned that we were not able to observe the radial breathing mode (RBM) in the Raman spectra, which would be a direct measure of the tube diameter.[16] Because the height of the CNT is on the order of 2 nm, this would correspond to a RBM frequency in the range of 100 cm^{-1}. In this spectral range, the intensity of the RBM Raman band becomes very weak[26] and additional instrumental factors such as Rayleigh scattering or absorption of the holographic Notch filter or both come into play. Therefore, in this study, we focus on the Raman spectroscopy of the D-line and G-lines in the frequency range between 1200 and 1700 cm^{-1}.

Because the Raman images in Figure 1c−f are based on the G-line intensity, the differences in Raman intensities directly

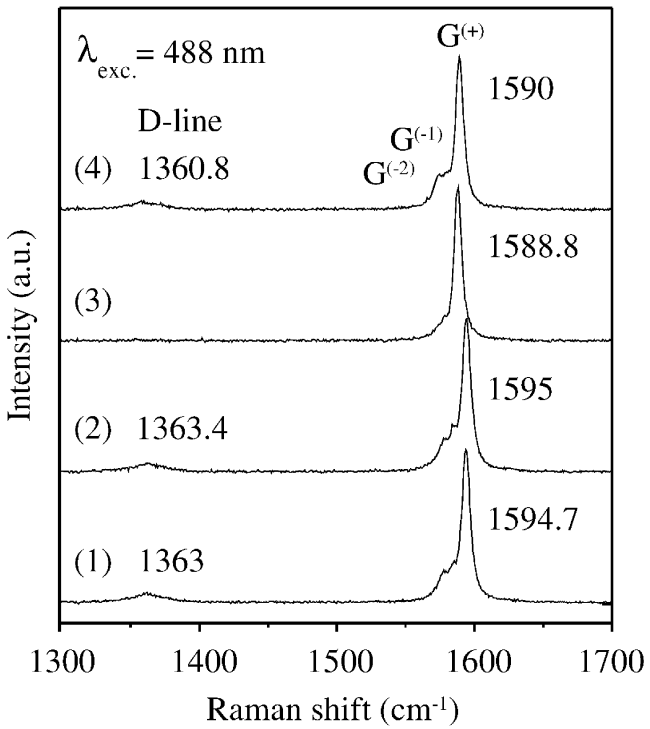

Figure 2. Raman spectra of the tube segments 1−4 in Figure 1 upon excitation with 488 nm. Segments 1, 2, and 4 show the D-line around 1360 cm^{-1} and three components of the G-line, while the D-line cannot be observed in segment 3. The spectral changes along the tube axis demonstrate the "electronic inhomogeneity" within the single CNT.

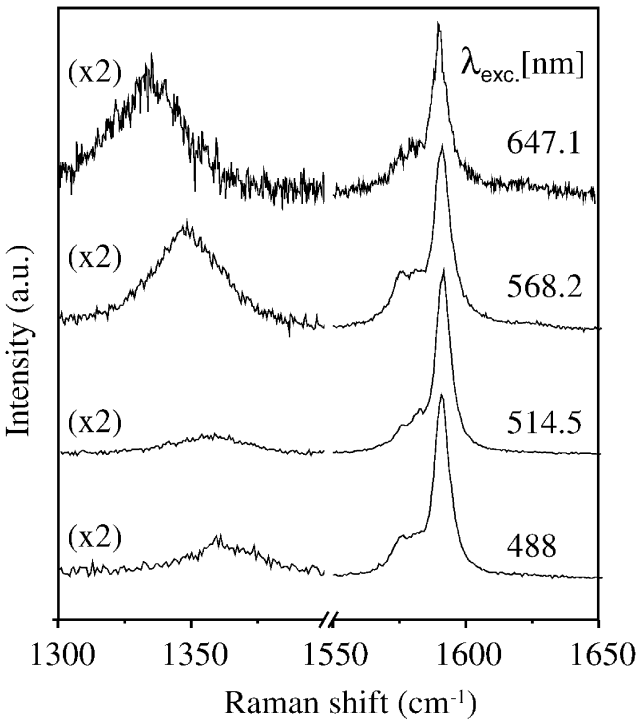

Figure 3. Raman spectra of tube segment 4 of Figure 1 upon excitation with four different wavelengths. While the shape and positions of the G-lines are similar at different excitation energies, the D-line is changing in its spectral position and relative intensity.

result from the different resonance conditions. Here the different excitation energies from 2.54 eV (488 nm) down to 1.92 eV (647.1 nm) cover several electronic transitions for tubes that are approx. 2 nm in diameter.[2] This could be, for example, the 3rd, 4th, or 5th electronic transition of semiconducting tubes (E_{sc}^{33}, E_{sc}^{44}, E_{sc}^{55}) or the 2nd transition of metallic tubes (E_{met}^{22}). However, because the CNT can in principle be seen at many wavelengths, absorption between the "tails" in the densities of state is obviously still sufficient to acquire Raman signals. In other words, the frequency selection for which different tubes within ensembles or bundles are "selectively excited" by different laser wavelengths just weights the intensity of different tubes but, in principle, shows only the average spectral properties.

Figure 2 shows the Raman spectra at different positions (1−4 in Figure 1) with an excitation wavelength of 488 nm. The spectra show the characteristic D- and the G-lines, which were fitted with one and three Lorentzian profiles, respectively. Obviously the band positions are slightly different even though the spectra belong to the same isolated CNT. Therefore, in addition to the intensity change, the difference in the Raman spectra is another indication that the structure of CVD-grown tubes changes along the tube axis.

A closer inspection of the G-line reveals that this band consists of at least three sharp bands with widths between 5 and 8 cm^{-1}, consistent with ref 26. The origin of these bands is still controversial. For example, it was claimed that the three components of the G-line ($G^{(-2)}$, $G^{(-1)}$, and $G^{(+)}$) correspond to Γ-point vibrations with different symmetries (E_1, A_1, and E_2).[27] Further, it was claimed that the splitting could be explained in combination with the longitudinal optical (LO) and transversal optical (TO) nature of those modes.[28] In a different explanation, it was assumed that the G-band does not correspond to phonon modes with a wave vector of $q = 0$ but rather originates from a double-resonance process that involves wave vectors of $q > 0$.[23]

A main difference between the single- and double-resonance process is that a dispersive effect should be experimentally observed for double resonances, that is, the spectral position of the bands should depend on the excitation energy. This (linear) frequency dependence was calculated for the D-line to be between 35 and 56 cm^{-1}/eV for different tube diameters.[20] For the G-lines, a *positive* frequency shift of approx. 3.5 cm^{-1}/eV independent of the tube chirality was calculated for the high-energy $G^{(+)}$-band, whereas a *negative* frequency shift was calculated for the low-energy $G^{(-)}$-mode, the magnitude of which should strongly depend on the tube chirality.[23]

With the single nanotube synthesized and characterized in this work, we have the ability to take Raman spectra of the different tube segments with various excitation wavelengths and compare the spectral evolutions with the theoretical predictions. For example, Figure 3 shows the Raman spectra taken with different excitation wavelength at position 4, that is, close to the top of the CNT loop, which could be clearly identified in the Raman images of four different excitation wavelengths. The spectra are normalized to the same G-line intensity, and the D-line is multiplied by a factor of 2 for clarity. It can clearly be seen that the position of the D-line is shifting to lower energies upon excitation with longer wavelength and that the relative intensity is increasing.[29] In principle, the relative intensity of the D-line is directly related to the number of defects and shows a complicated intensity and shape dependence upon excitation energy.[30] For the tube section 4, the relative D-line intensity (I_D/I_G) varied between 0.1 for $\lambda_{ex} = 488$ nm and 1 for $\lambda_{ex} = 647.1$ nm. However, for tube section 3 (see Figure 2), the D-line could hardly be observed. This indicates that also the density of defects of the CNT is changing along the tube axis.

In contrast to the D-line, Figure 3 reveals no detectable change of the G-line spectra upon excitation with different laser

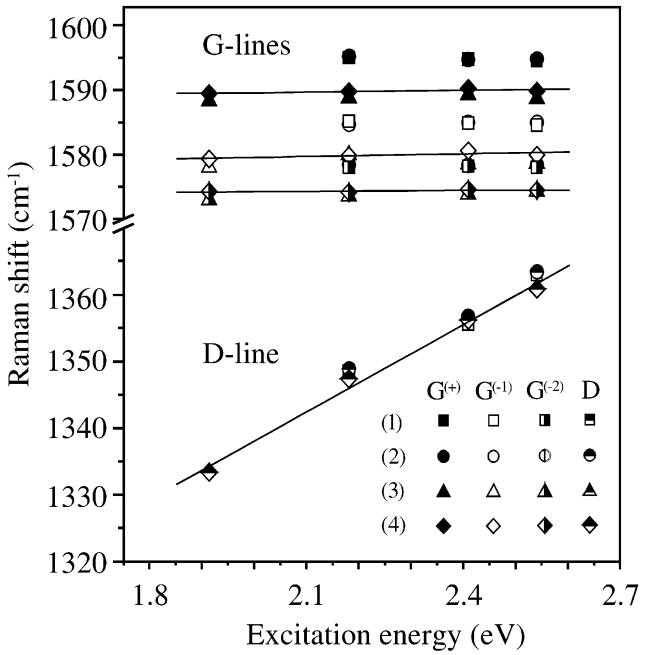

Figure 4. Excitation energy dependence of the G-line and D-line bands for the tube segments 1−4 in Figure 1. The solid lines show linear fits of the spectral evolutions for tube segment 4 (diamonds). The spectral positions of the G-bands change for different tube segments but are not dependent on the excitation wavelength within each segment. The spectral position of the D-line is almost similar for different tube segments but shows a linear dependence on excitation energy with a slope of 45−50 cm^{-1}/eV.

wavelength. For example, for the $G^{(+)}$-line, neither the shape (fwhm = 6.5−7.5 cm^{-1}) nor the spectral position (1589.8−1590.5 cm^{-1}) changes within the experimental error. This similarity reveals that we could not observe a dispersive effect for the G-line.

The spectral positions of the single Lorentzian fits of the D-line and the $G^{(+)}$-, $G^{(-1)}$-, and $G^{(-2)}$-lines for the different tube segments (1−4) as a function of excitation energy are summarized in Figure 4. The solid lines exemplify linear fits for the spectral evolution of tube segment 4. For the D-line, we could observe a linear dependence of the spectral positions on excitation energy with a slope of 49 ± 2.3, 45 ± 1.3, and 44 ± 1.3 cm^{-1}/eV for tube segments 1, 2, and 4, respectively, in accordance with various experimental results and theoretical predictions.[19,20,29] Also the spectral positions of the $G^{(+)}$- and $G^{(-)}$-bands are changing from one tube segment to another as discussed already. However, by comparing the spectral positions for the same tube segments, we could not observe a systematic shift with changing excitation energy.

In summary, we have grown isolated carbon nanotubes by CVD methods on substrates with patterned catalysts. The characteristic pattern allowed us to study the same isolated tube with AFM and confocal Raman spectroscopy. We could show that the Raman spectra change along the tube axis revealing that the tube is not uniform. Further, we could investigate the same tube segments with different excitation wavelengths to compare theoretically predicted frequency shifts for the D-line and the G-line. While the D-line showed a strong dispersive behavior of 45−50 cm^{-1}/eV, we could not observe a dependence of the G-line frequency on excitation energy.

Acknowledgment. We thank Dr. Marko Burghard for helpful discussion and Profs. Thomas Basché, Wolfgang Tremel, and Andreas Janshoff for experimental support. This work was supported by the BMBF under Contract Number 03C0302B9.

References and Notes

(1) Saito, R.; Dresselhaus, G.; Dresselhaus, M. S. *Physical Properties of Carbon Nanotubes*; Imperial College Press: London, 1998.
(2) Kataura, H.; Kumazawa, Y.; Maniwa, Y.; Umezu, I.; Suzuki, S.; Ohtsuka, Y.; Achiba, Y. *Synth. Met.* **1999**, *103*, 2555.
(3) Jiang, C.; Kempa, K.; Zhao, J.; Schlecht, U.; Kolb, U.; Basché, Th.; Burghard, M.; Mews, A. *Phys. Rev. B* **2002**, *66*, 161404.
(4) Cheung, C. L.; Kurtz, A.; Park, H.; Lieber, C. M. *J. Phys. Chem. B* **2002**, *106*, 2429.
(5) Kim, W.; Choi, H. C.; Shim, M.; Li, Y.; Wang, D.; Dai, H. *Nano Lett.* **2002**, *2*, 703.
(6) Franklin, N. R.; Dai, H. *Adv. Mater.* **2000**, *12*, 890.
(7) Ural, A.; Li, Y.; Dai, H. *Appl. Phys. Lett.* **2002**, *81*, 3464.
(8) Ouyang, M.; Huang, J.; Cheung, C.; Lieber, C. M. *Science* **2001**, *291*, 97.
(9) Mews, A.; Koberling, F.; Basché, Th.; Philipp, G.; Duesberg, G. S.; Roth, S.; Burghard, M. *Adv. Mater.* **2000**, *12*, 1210.
(10) Yu, Z.; Brus, L. E. *J. Phys. Chem. A* **2000**, *104*, 10995.
(11) Zhao, J.; Jiang, C.; Fan, Y.; Burghard, M.; Basché, Th.; Mews, A. *Nano Lett.* **2002**, *2*, 823.
(12) Yu, Z.; Brus, L. E. *J. Phys. Chem. B* **2001**, *105*, 1123.
(13) Hartschuh, A.; Sanchez, E. J.; Xie, S.; Novotny, L. *Phys. Rev. Lett.* **2003**, *90*, 095503.
(14) Dresselhaus, M. S.; Eklund, P. C. *Adv. Phys.* **2000**, *49*, 705.
(15) Yu, Z.; Brus, L. E. *J. Phys. Chem. B* **2001**, *105*, 6831.
(16) Jorio, A.; Saito, R.; Hafner, J. H.; Lieber, C. M.; Hunter, M.; McClure, T.; Dresselhaus, G.; Dresselhaus, M. S. *Phys. Rev. Lett.* **2001**, *86*, 1118.
(17) Jorio, A.; Souza, A. G.; Dresselhaus, G.; Dresselhaus, M. S.; Saito, R.; Hafner, J. H.; Lieber, C. M.; Matinaga, F. M.; Dantas, M. S. S.; Pimenta, M. A. *Phys. Rev. B* **2001**, *63*, 245416.
(18) Thomsen, C.; Reich, S. *Phys. Rev. Lett.* **2000**, *85*, 5214.
(19) Zólyomi, V.; Kürti, J.; Grüneis, A.; Kuzmany, H. *Phys. Rev. Lett.* **2003**, *90*, 157401.
(20) Maultzsch, J.; Reich, S.; Thomsen, C. *Phys. Rev. B* **2001**, *64*, 121407.
(21) Souza, A. G.; Jorio, A.; Samsonidze, G. G.; Dresselhaus, G.; Pimenta, M. A.; Dresselhaus, M. S.; Swan, A. K.; Unlu, M. S.; Goldberg, B. B.; Saito, R. *Phys. Rev. B* **2003**, *67*, 035427.
(22) Jorio, A.; Pimenta, M. A.; Souza, A. G.; Samsonidze, G. G.; Swan, A. K.; Unlu, M. S.; Goldberg, B. B.; Saito, R.; Dresselhaus, G.; Dresselhaus, M. S. *Phys. Rev. Lett.* **2003**, *90*, 107403.
(23) Maultzsch, J.; Reich, S.; Thomsen, C. *Phys. Rev. B* **2002**, *65*, 233402.
(24) Gu, G.; Philipp, G.; Wu, X.; Burghard, M.; Bittner, A. M.; Roth, S. *Adv. Funct. Mater.* **2001**, *11*, 295.
(25) Yang, P.; Zhao, D.; Margolese, D. I.; Chmelka, B. F.; Stucky, G. D. *Nature* **1998**, *396*, 152.
(26) Jorio, A.; Fantini, C.; Dantas, M. S. S.; Pimenta, M. A.; Souza, A. G.; Samsonidze, G. G.; Brar, V. W.; Dresselhaus, G.; Dresselhaus, M. S.; Swan, A. K.; Unlu, M. S.; Goldberg, B. B.; Saito, R. *Phys. Rev. B* **2002**, *66*, 115411.
(27) Saito, R.; Takeya, T.; Kimura, T.; Dresselhaus, G.; Dresselhaus, M. S. *Phys. Rev. B* **1998**, *57*, 4145.
(28) Saito, R.; Jorio, A.; Hafner, J. H.; Lieber, C. M.; Hunter, M.; McClure, T.; Dresselhaus, G.; Dresselhaus, M. S. *Phys. Rev. B* **2001**, *64*, 085312.
(29) Matthews, M. J.; Pimenta, M. A.; Dresselhaus, G.; Dresselhaus, M. S.; Endo, M. *Phys. Rev. B* **1999**, *59*, R6585.
(30) Kürti, J.; Zólyomi, V.; Grüneis, A.; Kuzmany, H. *Phys. Rev. B* **2002**, *65*, 165433.